PCCP

Accepted Manuscript

ROYAL SOCIETY OF CHEMISTRY

www.rsc.org/pccp

Bulk heterojunction organic solar cells based on carbazole-BODIPY conjugate small molecules as donor with high open circuit voltage

Thaksen Jadhav[1], Rajneesh Misra[1*], S. Biswas[2] and G. D. Sharma[3]*

[1]Department of Chemistry, Indian Institute of Technology Indore, Madhya Pradesh 452017, India
[2]Department of Physics, LNMIIT, Jaipur (Rajasthan) 302031, India
[3]R and D Center for Science and Engineering, JEC Group of Colleges, Jaipur Engineering College Campus, Kukas, Jaipur (Rajasthan), India

Abstract:

In this study, we have used three D-A type carbazole substituted BODIPY (carbazole connected to the meso position of BODIPY) small molecules as donors along with $PC_{71}BM$ as electron acceptor for the fabrication of solution processed bulk heterojunction organic solar cells. The devices based on as cast active layer showed power conversion efficiency in the range of 2.20–2.70%, with high open circuit voltage (V_{oc}) in the range of 0.94–1.08 V. The high V_{oc} is related to the deeper highest occupied molecular orbital energy level of these small molecules. The power conversion efficiency (PCE) of devices based on thermally annealed and solvent vapor annealed (TSVA) **3a**:$PC_{71}BM$ and **3c**:$PC_{71}BM$ processed active layer improved up to 5.05% and 4.80%, respectively, attributed to the improved light harvesting ability of active layers, better phase separation for exciton dissociation and balanced charge transport, induced by the TA and TSVA treatment.

Key words: Carbazole-BODIPY conjugate small molecules; Bulk heterojunction solar cells, Solvent vapor annealing; Power conversion efficiency.

* Corresponding authors e-mail address

G. D. Sharma (gdsharma273@gmail.com), Rajneesh Misra (rajneeshmisra@iiti.ac.in)

Introduction

In last couple of decades solution processable organic solar cells based on bulk heterojunction (BHJ) active layers have been extensively investigating due to light weight, low cost of fabrication and high power conversion efficiency (PCE).[1] The BHJ active layer used in these solar cells comprised fullerene derivatives such as [6,6]-phenyl-C_{61}-butyric acid methyl ester ($PC_{61}BM$) or [6,6]-phenyl-C_{71}-butyric acid methyl ester ($PC_{71}BM$), as electron-accepting materials, and various low band-gap π-conjugated polymers or small-molecules as the electron-donating materials. Recently, PCE of over 10% and 11% have been achieved for single BHJ layer and tandem solar cells, respectively.[2,3] The organic solar cells based on conjugated polymers as donors suffer from inherent disadvantages such as batch to batch variations, broad molecular weight distributions and many difficult steps for purification, which can rule out further improvement of overall performance and device stability.[4] On the other hand the conjugated small molecules (SMs) have well defined molecular structures and good batch to batch reproducibility, which makes them promising photovoltaic materials as an alternative to polymer donors. [5,6] The PCE of the solution processed organic BHJ based on D-A small molecules as donor has been reached in the range of 8-10%.[7]

Boron dipyrromethane (BODIPY) based dyes exhibit strong absorption and emission, thermally stable, and have strong acceptor nature.[8] Their photonic properties can be easily tuned by chemical transformation.[9] Carbazole derivatives have been extensively studied in optoelectronics owing to their low redox potential, hole transport property, and strong electron donating ability.[10,11] Employing the carbazole donating unit in D-A organic semiconductors, posses the deeper HOMO energy level, which leads to high open circuit voltage (Voc) in organic solar cells.[12] Zhang *et al* have reported that introduction of carbazole groups into the BODIPY unit improves the photonic properties resulting remarkable red shifted absorption spectra and better hole transport.[13] It was reported that inserting a π-linker

into D-A type molecular structure enhance the conjugation and coplanarity of organic semiconductors leading to the increased intramolecular charge transfer and short circuit current Jsc.[14]

Our research group has shown the effect of different functional groups at the β-pyrrolic position and meso-position of the BODIPY on its photonic properties.[15] Recently, we have synthesized three carbazole substituted BODIPY (carbazole connected to the meso position of BODIPY) small molecules and investigated their optical and electrochemical properties.[16] We found that the electron donating strength of the carbazole is directly function of the photophysical properties of carbazole –BODIPY conjugates and showed strong donor-acceptor interaction through the π-linker. Recently, Zhang et al have designed a star shaped carbazole –BODIPY derivates and used them as donor in BHJ organic solar cells and reported moderate PCE of 2.70% with high V_{oc} of 0.85 V.[17] Furthermore, ethynyl π- linker can increase the oxidation potential, hence increasing V_{oc}.[18] Recently, Liu *et al.* have reported a PCE of 3.13% for BODIPY based solution processed solar cells by dimerisation via the meso position.[19] Inspired by these excellent properties, we explored the possibilities of carbazole-BODIPY conjugate small molecules (chemical structures are shown in Scheme 1) for their possible application as donor material in solution processed BHJ organic solar cells. The *meso*-alkynylated BODIPYs are highly planar which is reflected from their crystal structure.[16] The high planarity ensures strong electronic communication between *meso* substituent and the BODIPY. There are no reports where carbazoles were substituted at *meso*-position of BODIPY *via* ethynyl linkage, which is being reported for solar cell applications. The carbazole substituted BODIPYs exhibits strong D-A character. The donor-acceptor (D-A) interaction in *meso* alkynylated BODIPY is better as compared to *α* and *β* -alkynylated BODIPYs.[15] The strong D-A interaction and absorption covering the entire UV-visible region make these molecules a promising candidate for the solar cell applications. The

BHJ solar cells based on these small molecules showed high V_{oc} in the range of 0.94 to 1.08 V, with overall PCE of 2.20 to 2.71% with as cast blend active layer. The PCE has been enhanced up to 5.05% and 4.80% using the TSVA processed **3a**:$PC_{71}BM$ and **3c**:$PC_{71}BM$ active layers, respectively. The enhanced PCE has been correlated to more favorable phase separation morphology, balanced charge transport, and light harvesting ability of the active layer, induced by the TSVA treatment.

Experimental details

Device fabrication and characterization

The solution processed BHJ organic solar cells with ITO/PEDOT:PSS/ active layer/Al were prepared as follow: The indium tin oxide (ITO) coated glass substrates were cleaned ultrasonically and subsequently in aqueous detergent, deionized water, isopropyl alcohol and acetone and finally dried under ambient conditions. An aqueous solution of PEDOT:PSS (Heraeus, clevious PVP, Al 4083) was spin cast on the ITO substrates to obtain a film with thickness of about 40 nm and dried for 10 min at a temperature of 120° C. Mixture of donor (**3a**, **3b** or **3c**) and $PC_{71}BM$ with weight ratios of 1:0.5, 1:1, 1:1.5, 1:2 and 1:2.5 in THF solution (concentration 10 mg/mL) were prepared and then spin cast onto the top of the PEDOT:PSS layer and dried at ambient conditions. The thickness of the active layer is about 85 nm ± 5 nm. Finally, the aluminum (Al) top electrode was thermally deposited on the top of active layer in a vacuum of 10^{-5} Torr through a shadow mask of 20 mm^2. All the devices were fabricated and tested under an ambient atmosphere without encapsulation. The hole-only and electron-only devices with ITO/PEODT:PSS/donor:$PC_{71}BM$/Au and ITO/Al/donor:$PC_{71}BM$/Al architectures were also fabricated in an analogous way, in order to measure the hole and electron mobility, respectively. The current-voltage (J-V) characteristics of the BHJ organic solar cells were measured using a computer controlled Keithley 238 source meter in dark as well as under simulated AM1.5G illumination of 100

mW/cm^2. A xenon light source coupled with optical filter was used to give the stimulated irradiance at the surface of the devices. The incident photon to current efficiency (IPCE) of the devices was measured illuminating the device through the light source and monochromator and the resulting current was measured using a Keithley electrometer under short circuit condition.

Results and discussions

Thermal, photophysical and electrochemical properties

The thermal stability is a key requirement for organic semiconductors for their application in optoelectronics devices. The thermogravimetric analysis (TGA) measurement at a heating rate of 10 °C/min under the nitrogen atmosphere was used to investigate the thermal properties of these small molecules. The decomposition temperature (T_d) for 10% weight loss in **3a**, **3b** and **3c** was estimated as 322, 360 and 368 °C, respectively (Table 1). The **3a** shows lower thermal stability may be due to the presence of alkyl groups and steric hindrance, whereas, **3b** and **3c** show similar thermal stability.

The normalized absorption spectra of **3a** and **3c** in DCM solution are shown in Figure 1 and the corresponding optical data are summarized in Table 1. Since **3b** shows similar absorption spectra to **3c**, we have not shown the absorption spectra of this molecule and only optical data are given in the Table 1. The carbazole-BODIPY conjugates **3a**-**3c** show a strong and sharp absorption band in the wavelength range of 530–550 nm with high molar extinction coefficient and also exhibits a pronounced shoulder in the 425–520 nm region. The **3a** shows an intramolecular charge transfer (ICT) band at round 595 nm, which may be exhibiting due to strong donor–acceptor interaction between the carbazole donor and BODIPY acceptor unit[20] as compared to **3b** and **3c**. The strength of the ICT band in these small molecule follows the trend as **3a**>**3c**>**3b**. The absorption spectra of **3a** and **3c** in thin film are shown in Figure 1. Compared to those in DCM solution, their absorption spectra in thin film become

broad and redshifted attributed to the intermolecular interaction between the molecules. The main absorption maxima are at 568 nm, 550 nm and 555 nm for **3a**, **3b** and **3c**, respectively. The ICT band of **3a** shifted to 620 nm. The optical bandgap of these molecules were estimated from the onset absorption edge of absorption spectra in thin film is about 1.75 eV, 1.94 eV and 1.90 eV, for **3a**, **3b,** and **3c**, respectively.

The electrochemical properties of these small molecules were investigated from the cyclic voltammetry and reported in our earlier report[16] and corresponding data are summarized in Table 2. The cyclic voltammogram reveals that the redox peaks are irreversible in nature. Small molecule **3a** shows two oxidation and reduction potential waves, whereas **3b** and **3c** show two oxidation and one reduction wave. The small molecule **3a** shows easier oxidation, indicating strong donor-acceptor interaction compared to **3b** and **3c.** The trend in the first oxidation potential follows the order **3b**>**3c**>**3a** and supports the strength of donor-acceptor interaction observed from the optical properties. The onset oxidation potential and onset reduction potential relative to the reference energy level of Fc/Fc^+ (4.40 eV below vacuum level) were used to estimate the HOMO and LUMO energy levels of these small molecules and are compiled in Table 2. In their negative potential region, these molecules exhibited similar onset reduction potential and LUMO levels are -3.44 eV, -3.44 eV, and -3.46 eV, for **3a**, **3b** and **3c**, respectively. Since the LUMO of D-A conjugated material is decided by the electron accepting strength of acceptor unit, identical LUMO of these molecules are attributed to the same BODIPY acceptor unit. The positive onset oxidation potentials of **3a**–**3c** are different and estimated values of HOMO energy levels are -5.48 eV, -5.54 eV and -5.62 eV for **3a**, **3b** and **3c**, respectively. The different HOMO level is attributed to the different electron donating ability of carbazole donors. The electrochemical bandgap are 2.04 eV, 2.10 eV and 2.16 eV, for **3a**, **3b** and **3c**, respectively. The trend of the electrochemical bandgap is similar to that obtained from optical data. The

LUMO energy levels of small molecules (**3a**, **3b** and **3c**) are suitable candidate to be used as electron donors when blended with $PC_{71}BM$ in BHJ organic solar cells. The deeper HOMO energy level of these small molecules is desirable for a high V_{oc}[21] and we expect high value of V_{oc}. The energy difference between the LUMO of these small molecules and $PC_{71}BM$ is higher than the exciton binding energy, indicating that efficient exciton dissociation in the D/A interface present in the active layer.

In order to get more information about the geometry and electronic structure of **3a**–**3c,** density functional theory calculations were carried out using the Gaussian 09Wprogram and reported in our earlier paper.[16] The theoretically estimated values of HOMO and LUMO are summarized in the Table 2. The trend of theoretical HOMO and LUMO energy levels and HOMO-LUMO gap is consistent with the experimentally observed values in cyclic voltammetry measurement.

Photovoltaic properties

In solution processed BHJ organic solar cells, the performance of device depends upon the relative amounts of the donor and acceptor materials employed in photoactive layer and there should be a balance between the absorbance and charge transport within the active layer. The electron transport will be limited, when active layer is too low, whereas the hole transport capability and absorbance in active layer will be decreased, when acceptor content is too high. In order to investigate the photovoltaic performance of three donors, devices based on conventional device structure of ITO/PEDOT:PSS/ active layer **3a** or **3b** or **3c** :$PC_{71}BM$/ Al were fabricated with various donor to acceptor weight ratios. The detail of fabrication procedure is given in the experimental section. Since **3b** and **3c** showed similar results, we have not included the figures for device based on **3b** and only given the data in Table 3. The weight ratio of donor and acceptor in active layer was optimized, and found D:A (1:2) is the optimized ratio of all three donors. We have chosen $PC_{71}BM$ instead of $PC_{61}BM$

as the acceptor since the former has a strong spectral absorption response in the visible region. Figure 2a and 3a show the current-voltage (J-V) characteristics of the best cells from the **3a** and **3c** as donor under the optimized D:A weight ratio and the corresponding photovoltaic parameters are summarized in Table 3. The higher value of PCE for **3a**:$PC_{71}BM$ (2.71 % with J_{sc} =7.58 mA/cm^2, V_{oc} =0.94 V and FF= 0.38) active layer as compared to **3b**:$PC_{71}BM$ (2.24 % with J_{sc} = 6.10 mA/cm^2, V_{oc} = 1.08 V and FF= 0.34) and **3c**:$PC_{71}BM$ (2.20 % with J_{sc} = 6.22 mA/cm^2, V_{oc} = 1.04 V and FF = 0.34) has been attributed to the higher values of J_{sc} and FF. The value of V_{oc} for **3b** (1.08 V) and **3c** (1.04V) based devices is higher as compared to **3a** (0.94 V), may be attributed to the deeper HOMO levels of **3b** and **3c**, as the V_{oc} in the BHJ organic solar cells is directly related to the energy difference between the HOMO level of donor and LUMO level of acceptor materials used in BHJ active layer. Still higher V_{oc} can be achieved if the recombination of charge carrier can be suppressed.[22] In order to verify the accuracy of the values of J_{sc} derived from the J-V characteristics, the corresponding IPCE spectra of the devices were measured and shown in Figure 2b and 3b. The IPCE values are higher for the device based on **3a** in the entire wavelength region as compared to that for **3c** and closely resembles with the corresponding absorption spectra of the active layer. The J_{sc} values calculated from the integration of the IPCE spectra was 7.38 mA/cm^2 and 5.96 mA/cm^2 for **3a** and **3c** based devices, respectively, which agree well with the J_{sc} values estimated from J-V measurements. Although the absorption near 700 nm is weak, the IPCE value is attributed to the fact that in longer wavelength region, the electronic transitions are capable of transformation with sufficient efficiency of photons to electrons. The higher value of J_{sc} for **3a** based device may be attributed to the better absorption profile of active layer and low bandgap and higher hole mobility of donor.[23]

In addition to the optical absorption and energy levels of the donor material, used in active layer, charge carrier mobilities and balance charge transport are crucial factors for achieving high PCE. We have estimated the hole mobility of donors **3a** and **3c** in the active layers using the J-V characteristics of the hole only devices ITO/PEDOT:PSS/active layer/Au employing the space charge limited current model.[24] As shown in Figure 4, the hole mobilities were calculated as 7.84 x10^{-6} cm^2/Vs and 3.68 x10^{-6} cm^2/Vs for **3a** and **3c**, respectively. It is well known that the charge transport is limited by the thickness of the active layer. If the thickness is very small, than the FF will improve but the light harvesting ability of the active layer will reduced. Although the thickness of the active layer influences the charge carrier mobility, and we took much care to ensure alike film thickness of the active layer (85 nm ± 5 nm) and avoid substantial influence of this parameter on the devices' charge mobility. The higher hole mobility for **3a** illustrates that structural modification of carbazole unit has been extended efficiently and its charge transport ability has improved. These results show that hole mobility of **3a** is higher than that for **3c** and may be one of the potential reason for the fact that **3a**:$PC_{71}BM$ based device exhibit higher J_{sc} and FF than that for **3c** based devices.

In order to understand the intermolecular interchain and molecular packing, XRDs were also recorded for the films of **3a** and **3c** and shown in Figure 5. Two sharp different peaks were observed in the small angle region, i.e. 2θ = 4.58° and 2θ= 4.86° for **3c** and **3a**, respectively, were corresponding to interchain d-spacing of 20.16 A and 18.24 A, respectively. The shorter interchain distance indicates that molecules pack closer by inter-digitizing the side chain. The stronger diffraction peak intensity for **3a** is likely related to its high degree of crystallinity. Moreover, a broad peak in the wider angle (2θ = 20-25°) is displayed of both **3a** and **3c**, which is ascribed to the interlayer π-π stacking of the main chain. The higher crystallinity for **3a** would increase the intermolecular interaction and facilitates charge carrier mobility and resulted enhancement in the J_{sc} and PCE.

The devices based on active layer using these three donors processed without any treatment exhibited low PCE in the range of 2.20 -2.71 %. Although the V_{oc} for these devices is quite high but the poor PCE is mainly related to the low values of both J_{sc} and FF. The relative low hole mobility and mismatch between the electron and hole mobilities may also attributed to the low value of FF in these devices and may also be a factor which limits the J_{sc} of the BODIPY based small molecule devices.[24, 25] The low values of FF and J_{sc} may also be related to poor nanoscale morphology of the active layer for exciton dissociation and charge transport. In the solution processed BHJ organic solar cell, the absorption of photons by the active layer produces an exciton which must be dissociated into free charge carriers at the donor/acceptor interface present within the active layer. The morphology and phase separation between the donor and acceptor materials should be within the range of exciton diffusion length otherwise the exciton will be lost during their transportation towards the D/A interface.[26] Therefore, the exciton dissociation and charge transport strongly depends upon the optimized nanoscale morphology and phase separation of the BHJ active layer. In order to improve the morphology of the active layer, strategies such as thermal annealing and use of solvent additives and solid additives have been reported.[27] In addition to above, solvent vapor annealing treatment can also help to form the crystalline domains and suitable for ambient conditions and improves the overall PCE of the solution processed organic solar cells.[28, 29] We have used the two step treatment i.e., thermal annealing (TA) treatment followed by the solvent vapor annealing (SVA) treatment for **3a** and **3c** BODIY small molecules. In the case of thermal annealing the optimized active layer was thermally annealed at 110 °C for 10 min. For SVA treatment, the active layer was exposed to chloroform vapor for 60 s after the TA treatment. This strategy has been found most suitable to achieve the high PCE for solution processed small molecule organic solar cells.[30,7e] For this, first, the BHJ active layer as cast from THF solution onto the PEDOT:PSS layer was heated on a hotplate at 110° C for 1o

minutes. After cooling to room temperature, the film was placed on a Petri dish containing 200 μL chloroform for solvent vapor annealing for 60s. The J-V characteristics of the devices with TA and TSVA are shown in Figure 2a and 3a for **3a** and **3c**, respectively. After thermal annealing (TA), the devices based on **3a** and **3c** exhibited PCE of 3.99 % (J_{sc} = 9.24 mA/cm^2, V_{oc} = 0.90 V and FF= 0.48) and 3.56 % (J_{sc}= 8.52 mA/cm^2, V_{oc} = 0.98 and FF= 0.45), respectively. After the TSVA treatment, the performance PCE was further improved up to 5.05 % (J_{sc} = 10.20 mA/cm^2, V_{oc} = 0.90 V and FF= 0.55) and 4.80 % (J_{sc} =9.64 mA/cm^2, V_{oc} = 0.96 V and FF = 0.52), for **3a** and **3c** based devices, respectively. It was observed that the V_{oc} of the devices slightly lower for devices with active layer treated with either TA or TSVA treatment. The TA and TSVA treatment leads to increase the interaction between the donor and acceptor thereby influences the reverse saturation current, leading to decrease the V_{oc}.[31] The increase in J_{sc} and FF may be originated from the enhanced absorption, better nanoscale morphology of active layer and more balanced charge transport, induced by the TA and TSVA treatments. The further increase in J_{sc} with TSVA treatment is attributed to the fact that solvent vapor can penetrate into the film, allowing the molecules to reorganize for a more ordered packing structures.

In order to get information about the enhancement in the J_{sc}, we have measured the IPCE spectra of devices with TA and TSVA treated BHJ active layer and shown in Figure 2b and 3b. The IPCE spectra of the devices based on TA and TSVA treated active layer shows higher values of IPCE throughout the whole wavelength region of measurements. Since the J_{sc} of the BHJ organic solar cell depends upon the light harvesting ability of active layer, we have measured the absorption spectra of BHJ active layer with TA and TSVA treatment and as cast. As shown in Figure 6a (for **3a**) and 4b (for **3c**), in comparison with the spectra of as cast active layer, the spectra of the devices processed with TA shows a red shift and intensity also increased. For the active layer films with further SVA treatment, the overall absorption

intensity increased and thus resulting in improved J_{sc}. The IPCE spectra of devices closely resemble with the corresponding absorption spectra of the active layers. The calculated J_{sc} obtained from the integration of IPCE spectra are 9.12 mA/cm^2 (TA for **3a**), 10.08 mA/cm^2 (TSVA for **3c**), 8.44 mA/cm^2 (TA for **3c**) and 9.52 mA/cm^2 (for TSVA for **3c**), and are closely in agreement with the J_{sc} value obtained from the J-V characteristics.

The surface morphology of the **3a**:$PC_{71}BM$ thin film processed as cast, TA and TSVA treatments were investigated by transmission electron microscopy (TEM) shown in Figure 7. It can be seen from these images that TA processed film showed better phase separation as compared to as-cast film and further improved with TSVA treatment. The better nanoscale phase separation and bicontinuous interpenetrating network contributes to the high exciton dissociation and charge transport efficiency resulting in enhancement in J_{sc}, FF and PCE.[25]

Moreover, the crystallinity of active layer is another factor which also affects the charge transport and light harvesting efficiency of the device, thereby affecting the overall performance of BHJ organic solar cells. To get the information about the change in crystallinity of blended active layers processed under different treatments, we have recorded their XRD patterns and shown in Figure 5b (for **3a**:$PC_{71}BM$ only). Similar XRD patterns were also observed for **3c:**$PC_{71}BM$ thin films. The cast **3a**:$PC_{71}BM$ film shows a relatively broad and weak diffraction peaks as compared to the pristine **3a** film at 2θ=4.86°, corresponding to the crystalline domains of **3a**. However, in the TA processed film, this diffraction peak becomes narrower as well as more intense. Moreover, the full width at half maxima (FWHM) also reduced. These effects indicate that the increase in the ordered crystallinity of **3a** in the TA treated blend as compared to as cast counter part. The intensity of the diffraction peak is seen to further increase with subsequent SVA, i.e.TSVA treatment, leading to further increase in the crystalline nature of the blend. The observed increase in crystalline nature between the active layers processed as cast and those with additional

treatments is consistent with the significant increase in FF. The overall increase in order of the molecular packing improves the IPCE values and is likely to be responsible for increase in J_{sc} and PCE.

In order to further demonstrate that the simultaneous improved charge transport ability and their balance in the active layer, we have measured the hole mobility in the active layer, processed with different treatment, from the J-V characteristics of the hole only devices in dark (Figure 4a and 4b) and using SCLC model. For the TA based devices, the hole mobility increased up to $5.34x10^{-5}$ cm^2/Vs and $1.21x10^{-5}$ cm^2/Vs for **3a**:$PC_{71}BM$ and **3c**:$PC_{71}BM$, respectively. Additionally, the device based on TSVA processed **3a**:$PC_{71}BM$ and **3c** $PC_{71}BM$ exhibit a higher hole mobility $8.45x10^{-5}$ cm^2/Vs and 5.48 cm^2/Vs with much more balanced charge transport as shown in Table 3. The balanced charge transport is beneficial for improved FF. The decrease in series resistance (R_s) and increase in shunt resistance (R_{sh}), as shown in Table 3, are responsible for increase in J_{sc} and FF in the devices based on the TA and TSVA treated active layers. Although the PCE of the devices have be significantly improved after the TA and TSVA treatments but the FF is still low. The reasons for low FF obtained in small molecule donor materials has been previously described by Marks et al. [32] and shown that charge carrier extraction at the contacts had been key to improve the FF of small molecule donor based organic solar cells. In particular, adequate energy level alignment is a requirement to ensure good extraction. Since the HOMO energy levels of these small molecules is quite deeper than PEDOT:PSS (5.0-5.2 eV), the extraction of the holes is not so efficient. It is quite possible that other hole selective layers like MoO_3 may be beneficial to improve the contact. The same applies for the low WF contact such as Al contact which has been processed in air (and measured) and it is known that a thin layer of Al_2O_3 may be generating under this conditions reducing the extraction ability.

Conclusions

In summary, we have employed three carbazole substituted BODIPY (carbazole connected to the meso position of BODIPY) small molecules as donor along with the $PC_{71}BM$ as electron acceptor for the fabrication of solution processed BHJ solar cells. The BHJ based on these small molecules showed quite high V_{oc} in the range of 0.94- 1.08 V, with overall PCE in the range of 2.20 to 2.71 % with as cast active layers. The high V_{oc} attributed to the deeper HOMO levels of these small molecules. The PCE solar cells of **3a**:$PC_{71}BM$ and **3c**:$PC_{71}BM$ active layer processed with TSVA further improved up to 5.05 % and 4.80 %, respectively. The increase in PCE has been attributed to the enhancement in J_{sc} and FF, related to the better phase separation, improved light harvesting ability of active layer and more balanced charge transport, induced by the TSVA treatment.

References

1 (a) S. Few, J. M. Frost and J. Nelson, *Phys. Chem. Chem. Phys.*, 2015, **17**, 2311; (b) G. Lakhwani, A. Rao and R. H. Friend, *Annu. Rev. Phys. Chem.*, 2014, **65**, 557; (c) S. Gelinas, A. Rao, A. Kumar, S. L. Smith, A. W. Chin, J. Clark, T. S. van der Poll, G. C. Bazan and R. H. Friend, *Science,* 2014, **343**, 512; (d) C. Groves, *Energy Environ. Sci.*, 2013, **6**, 1546; (e) M. L. Jones, R. Dyer, N. Clarke and C. Groves, *Phys. Chem. Chem. Phys.*, 2014, **16**, 20310.

2 (a) Y. Liu, J. Zhao, Z. Li, C. Mu, W. Ma, H. Hu, K. Jiang, H. Lin, H. Ade and H. Yan, *Nat. Commun.*, 2014, **5**, 5293; (b) Z. C. He, C. M. Zhong, S. J. Su, M. Xu, H. B. Wu and Y. Cao, *Nat. Photonics*, 2012, **6**, 591–595; (c) M. Wang, X. W. Hu, P. Liu, W. Li, X. Gong, F. Huang and Y. Cao,*J. Am. Chem. Soc.*, 2011, **133**, 9638–9641; (d) W. Li, A. Furlan, K. H. Hendriks, M. M. Wienk and R. A. J. Janssen, *J. Am. Chem. Soc.*, 2013, **135**, 5529–5532; (e) J. You, L. Dou, K. Yoshimura, T. Kato, K. Ohya, T. Moriarty, K. Emery, C.-C. Chen, J. Gao, G. Li and Y. Yang, *Nat. Commun.*, 2013, **4**, 1446–1453.

3 C. C. Chen, W.H. Chang, K. Yoshimura, K. Ohya, J. You, J. Gao, Z. Hong and Y. Yang, *Adv. Mater.*, 2014, **26**, 5670–5677; (b) A. R. B. Mohd Yusoff, D. Kim, H. P. Kim, F. K. Shneider, W. J. da Silva and J. Jang, *Energy Environ. Sci.*, 2015, **8**, 303–316.

4 (a) H. Burckstummer, N. M. Kronenberg, M. Gsanger, M. Stolte, K. Meerholz and F. Wurthner, *J. Mater. Chem.*, 2010, **20**, 240–243; (b) J. Roncali, *Acc. Chem. Res.*, 2009, **42**, 1719–1730; (c) B. Walker, A. B. Tamayo, X.-D. Dang, P. Zalar, J. H. Seo, A. Garcia, M. Tantiwiwat and T.-Q. Nguyen, *Adv. Funct. Mater.*, 2009, **19**, 3063–3069.

5 (a) J. E. Coughlin, Z. E. Henson, G. C. Welch and G. C. Bazan, *Acc. Chem. Res.*, 2014, **47**, 257–270; (b) Y. Chen, X. Wang and G. Long, *Acc. Chem. Res.*, 2013, **46**, 2645–2655; (c) B. Walker, C. Kim and T.-Q. Nguyen, *Chem. Mater.*, 2011, **23**, 470–482; (d) A. Mishra and P. Bauerle, *Angew. Chem. Int. Ed.*, 2012, **51**, 2020–2067; (e) Y. Lin, Y. Li and X. Zhan, *Chem. Soc. Rev.*, 2012, **41**, 4245–4270; (f) J. Roncali, P. Leriche and P. Blanchard, *Adv. Mater.*, 2014, **26**, 3821–3838.

6 (a) V. Malytskyi, J.-J. Simon, L. Patrone and J.-M. Raimundo, *RSC advance*, 2015, **5**, 354-397, (b) W. Ni, X. Wan, M. Li, Y. Wang and Y. Chen, *Chem. Commun.*, doi: 10.1039/c4cc09758k; (c) M. Li, W. Ni, X. Wan, Q. Zhang, B. Kan and Y. Chen, *J. Mater. Chem. A*, doi: 10.1039/c4ta06452f.

7 (a) A. K. Kyaw, D. H. Wang, D. Wynands, J. Zhang, T. Q. Nguyen, G. C. Bazan, A. J. Heeger, *Nano Lett.*, 2013, **13**, 3796; (b) B. Kan, Q. Zhang, M. Li, X. Wan, W. Ni, G. Long, Y. Wang, X. Yang, H. Feng, Y. Chen, *J. Am. Chem. Soc.*, 2014, **136**, 15529; (c) Y. Liu, C. C. Chen, Z. Hong, J. Gao, Y. M. Yang, H. Zhou, L. Dou, G. Li and Y. Yang, *Sci. Rep.*, 2013, **3**, 3356; (d) Q. Zhang, B. Kan, F. Liu, G. Long, X. Wan, X. Chen, Y. Zuo, W. Ni, H. Zhang, M. Li, Z. Hu, F. Huang, Y. Cao, Z. Liang, M. Zhang, T. P. Russell and Y. Chen, *Nat. Photonics*, 2015, **9**, 35; (e) B. Kan, M. Li, Q.

Zhang, F. Liu, X. Wan, Y. Wang, W. Ni, G. Long, X. Yang, H. Feng, Y. Zuo, M. Zhang, F. Huang, Y. Cao, T. P. Russell and Y. Chen, *J. Am. Chem. Soc.*, 2015, **137**, 3886-3893.

8 (a) A. Loudet and K. Burgess, *Chem. Rev.*, 2007, **107**, 4891; (b) G. Ulrich, R. Ziessel and A. Harriman, *Angew. Chem., Int. Ed.*, 2008, **47**, 1184.

9 (a) O. A. Bozdemir, R. Guliyev, O. Buyukcakir, S. Selcuk, S. Kolemen, G. Gulseren, T. Nalbantoglu, H. Boyaci and E. U. Akkaya, *J. Am. Chem. Soc.*, 2010, **132**, 8029; (b) M. E. El-Khouly, S. Fukuzumi and F. D'Souza, *ChemPhysChem*, 2014, **15**, 30–47; (c) A. Loudet and K. Burgess, *Chem. Rev.*, 2007, **107**, 4891–4932; (d) A. Bessette and G. S. Hanan, *Chem. Soc. Rev.*, 2014, **43**, 3342.

10 (a) X. Zhang, Y. Xiao, J. Qi, J. Qu, B. Kim, X. Yue and K. D. Befield, *J. Org. Chem.*, 2013, **78**, 9153; (b) D. Zhang, V. Martın, I. Garcıa-Moreno, A. Costela, M. E. P´erez-Ojeda and Y. Xiao, *Phys. Chem. Chem. Phys.*, 2011, **13**, 13026.

11 (a) J. V. Grazulevicius, P. Strohriegl, J. Pielichowski and K. Pielichowski, *Prog. Polym. Sci.*, 2003, **28**, 1297; (b) J. F. Morin, M. Leclerc, D. Adès and A. Siove, Macromol. *Rapid Commun.*, 2005, **26**, 761; (c) N. Blouin and M. Leclerc, *Acc. Chem. Res.*, 2008, **41**, 1110; (d) S. Sujeewa, X. C. Palayangoda, R. M. Adhikari and D. C. Neckers, *Org. Lett.*, 2008, **10**, 4; (e) J. Li and A. C. Grimsdale, *Chem. Soc. Rev.*, 2010, **39**, 2399.

12 (a) N. Blouin, A.Michaud, D. Gendron, S. Wakim, E. Blair, R. Neagu-Plesu, M. Belletete, G. Durocher, T. Tao and M. Leclerc, *J. Am. Chem. Soc.* 2008, **130**, 732; (b) R. Qin, W. Li, C. Li, C. Du, C. Viet, H.F. Schleiermacher, M. Andersson, Z. Bo, Z. Liu, O. Inganas, U. Wuerfel and F. Zhang, *J. Am. Chem. Soc.*, 2009, **131**, 14612; (c) S. H. Park, A. Roy, S. Beaupre, S. Cho, N. Coates, J.S. Moon, D. Moses, M. Leclerc, K. Lee and A, J. Heeger, *Nat. Photonics*, 2009, **3**, 297.

13 (a) X. Zhang, Y. Xiao, J. Qui, J. Qu, B. Kim, X. Yue, and K. D. Belfield, *J. Org. Chem.*, 2013, **78**, 9173; (b) D. Zhang, V. Martin, I. Garcia-Moreno, A. Costela, M. E. Perez-Qjeda and Y. Xiao, *Phys. Chem. Chem. Phys.*, 2011, **13**, 13026.

14 (a) J. Zhang, Y. Yang, C. He, Y. He, G. Zhao and Y. Li, *Macromolecules*, 2009, **42**, 7619; (c) A. L. Kanibolotsky, F. Vilela, J. C. Forgie, S. E. T. Elmasly, P. J. Skabara, K. Zhang, B. Tieke, J. McGurk, C. R. Belton, P. N. Stavrinou and D. D. C. Bradley, *Adv. Mater.*, 2011, **23**, 2093.

15 (a) R. Misra, B. Dhokale, T. Jadhav and S. M. Mobin, *Dalton Trans.*, 2013, **42**, 13658; (b) P. Gautam, B. Dhokale, S. M. Mobin and R. Misra, *RSC Adv.*, 2012, **2**, 12105-12107; (c) R. Misra, B. Dhokale, T. Jadhav and S. M. Mobin, *Organometallic*, 2014, **33**,1867-1877; (d) B. Dhokale, P. Gautam, S. M. Mobin and R. Misra, *Dalton Trans.*, 2013, **42**, 1512-1518; (e) B. Dhokale, T. Jadhav, S. M. Mobin and R. Misra, *Chem. Commun.*, 2014, **50**, 9119-9121.

16 R. Misra, T. Jadhav, B. Dhokale, P. Gautam, R. Sharma, R. Maragani and S. M. Mobin, *Dalton Trans.,* 2014, **43**, 13076.

17 X. Zhang, Y. Zhang, L. Chen and Y. Xiao, *RSC Adv.*, 2015, **5**, 32283-32289.

18 S. Zang, L. Yin, C. Ji, X. Jiang, K. Li, Y. Li and Y, Wang, *Chem. Comm.*, 2012, **48**, 10627.

19 W. Liu, A. Tang, J. Chen, Y. Wu, C. Zhan and J. Yao, *ACS Appl. Mater. Interfaces*, 2014, **6**, 22496-22505.

20 (a) W. Qin, M. Baruah, M. van der Auweraer, F. C. De Schrywer and N. Boens, *J. Phys. Chem. A*, 2005, **109**, 7371-7384; (b) E. Larger, J. Liu, A. Aguilar-Aguilar, B. Z. Tang and E. Pena-Cabrerra, *J. Org. Chem.*, 2009, **74**, 2053.

21 (a) J. Hou, Z. Tan, Y. Yan, Y. He, C. Yang and Y. Li, *J. Am. Chem. Soc.*, 2006, **128**, 4911; (b) Y. He, H. Y. Chen, J. Hou and Y. Li, *J. Am. Chem. Soc.*, 2010, **132**, 1377,

(c) M. C. Scharber, D. Mühlbacher, M. Koppe, P. Denk, C. Waldauf, A. J. Heeger, A. J., C. J. Brabec, *Adv. Mater.,* 2006, **18**, 789–794.

22 (a) J. Bisquert, G. Garcia,-Belmonte, *J. Phys. Chem. Lett.* 2011, **2**, 1950-1964, (b) A. Guerreno, N. F. Montcada, J. Ajuria, I. Etxebarria, R. Pacios, G. Garcia-Belmonte, E. Palomares, *J. Mater. Chem. A* 2013, **1**, 12345-12354

23 (a) Y. J. Cheng, S. H. Yang and C. S. Hsu, *Chem. Rev.*, 2009, **109**, 5868–5923; (b) H. Shang, H. Fan, Y. Liu, W. Hu, Y. Li and X. Zhan, *Adv. Mater.*, 2011, **23**, 1554–1557; (c) Y. Lin, L. Ma, Y. F. Li, Y. Liu, D. Zhu and X. Zhan, *Adv. Energy Mater.*, 2013, **3**, 1166–1170.

24 V. Mihailetchi, J. Wildeman and P. Blom, *Phys. Rev. Lett.*, 2005, **94**, 126602.

25 H. Kang, S. Y. An, B. Walker, S. Song, T. Kim, J. Y. Kim, C. Yang, *J. Mater. Chem. A*, doi: 10.1039/c5ta00016e.

26 C. M. Proctor, M. Kuik and T .Q. Nguyen, *Prog. Polym. Sci.*, 2013, **38**, 1941-1960.

27 (a) W. Shin, T. Yasuda, G. Watanabe, Y. S. Yang and C. Adachi, *Chem. Mater.*, 2013, **25**, 2549–2556; (b) K. R. Graham, R. Stalder, P. M. Wieruszewski, D. G. Patel, D. H. Salazar and J. R. Reynolds, *ACS Appl. Mater. Interfaces*, 2013, **5**, 63–71; (c) J. Huang, C. Zhan, X. Zhang, Y. Zhao, Z. Lu, H. Jia, B. Jiang, J. Ye, S. Zhang, A. Tang, Y. Liu, Q. Pei and J. Yao, *ACS Appl. Mater. Interfaces*, 2013, **5**, 2033–2039; (d) H. Wang, F. Liu, L. Bu, J. Gao, C. Wang, W. Wei and T. P. Russell, *Adv. Mater.*, 2013, **25**, 6519–6525; (e) K. R. Graham, P. M. Wieruszewski, R. Stalder, M. J. Hartel, J. Mei, F. So and J. R. Reynolds, *Adv. Funct. Mater.*, 2012, **22**, 4801–4813; (g) J. Zhou, X. Wan, Y. Liu, Y. Zuo, Z. Li, G. He, G. Long, W. Ni, C. Li, X. Su and Y. Chen, *J. Am. Chem. Soc.*, 2012, **134**, 16345-16351; (h) H. C. Liao, C. C. Ho, C. Y. Chang, M. H. Jao, S. B. Darling, W. F. Su, *Mater. Today*, 2013, **16**, 326-336; (j) F. Machui, P.

Maisch, S. Langner, J. Krantz, T. Ameri and C. J. Brabec, *ChemPhysChem* doi:10.1002/cphc.201402734.

28 (a) M. T. Lloyd, A. C. Mayer, S. Subramanian, D. A. Mourey, D. J. Herman, A. V. Bapat, J. E. Anthony and G. G. Malliaras, *J. Am. Chem. Soc.*, 2007, **129**, 9144–9149; (b) G. H. Lu, L. G. Li and X. N. Yang, *Adv. Mater.*, 2007, **19**, 3594–3598; (c) J. Vogelsang, J. Brazard, T. Adachi, J. C. Bolinger and P. F. Barbara, *Angew. Chem., Int. Ed.*, 2011, **50**, 2257–2261; (d) K. Sun, Z. Xiao, E. Hanssen, M. F. G. Klein, H. H. Dam, M. Pfaff, D. Gerthsen, W. W. H. Wong and D. J. Jones, *J. Mater. Chem. A,* doi: 0.1039/c4ta01125b.

29 (a) H. Tang, G. Lu, L. Li, J. Li, Y. Wang and X. Yang, *J. Mater. Chem.*, 2010, **20**, 683–688; (b) G. Wei, S. Wang, K. Sun, M. E. Thompson and S. R. Forrest, *Adv. Energy Mater.*, 2011, **1**, 184–187.

30 (a) C. D. Wessendorf, G. L. Schulz, A. Mishra, P. Kar, I. Ata, M. Weidelener, M. Urdanpilleta, J. Hanisch, E. Lindén, M. Mena-Osteritz, E. Ahlswede, P. Bä uerle, *Adv. Energy Mater.*, 2014, **4**, 1400266; (b) B. Kan, Q. Zhang, M. Li, X. Wan, W. Ni, G. Long, Y. Wang, X. Yang, H. Feng and Y. Chen, *J. Am. Chem. Soc.* doi: 10.1021/ja509703k; (c) W. Ni, M. Li, X. Wan, H. Feng, B. Kan, Y. Zuo and Y. Chen, *RSC Adv.*, 2014, **4**, 31977.

31 G. Long, X. Wan, B. Kan, Y. Liu, G. He, Z. Li, Y. Zhang, Y. Zhang, Q. Zhang, M. Zhang and Y. Chen, *Adv. Energy Mater.*, 2013, **3**, 639–646.

32 A. Guerrero, S. Loser, G. Garcia-Belmonte, C. J. Bruns J. Smith, H. Miyauchi, S. I. Stupp, J. Bisquert, T. J. Marks, *Phys. Chem. Chem. Phys.,* 2013 **15**, 16456-16462

Table 1. Photophysical (DCM solvent) and thermal properties of BODIPYs **3a-3c**.

BODIPY	λ_{abs}(nm)a ($\varepsilon\times10^4$ (mol^{-1} cm^{-1})	λ_{abs}(nm)[b]	Optical band gap (eV)[c]	T_d[d] (°C)
3a	584 (1.78) 540 (5.85)	614	1.72	322
3b	541 511 481	586	1.88	366
3c	537 504	578	1.85	368

[a]in DCM solution, [b]thin film cast from DCM, [c]estimated from the onset absorption edge in the absorption spectra observed in thin film cast from DCM, [d]Decomposition temperature at 10% weight loss, determined by TGA

Table 2. Electrochemical properties and theoretical values of HOMO and LUMO levels of the BODIPYs 3a-3c.[a]

BODIPY	$E^1_{oxid}(V)$ [a]	$E^2_{oxid}(V)$ a	$E^1_{red}(V)$ [a]	$E^2_{red}(V)$[a]	E_{HOMO}/E_{LUMO} eV)[b]	E_{HOMO}/E_{LUMO} (eV)[c]
3a	1.16	1.54	-0.63	-0.95	-5.48/-3.44	-5.56/2.97
3b	1.24	1.77 (broad)	-1.34	-	-5.62/-3.42	-5.76/-2.96
3c	1.21	1.58 (broad)	-1.16	-	-5.54/-3.46	5.67/-2.83

[a]electrochemical analysis was performed, in 0.1 M solution of Bu_4NPF_6 in DCM at 100 mV s^{-1} scan rate, versus Fc/Fc^+. [b]irreversible wave, [b]E_{HOMO} / E_{LUMO} = -(E_{onset}-4.4)eV, [c]Theoretical values calculated from DFT

Table 3. Photovoltaic parameters of the solution processed BHJ solar cells based on **3a-3c** :$PC_{71}BM$ active layers processed under different treatments.

Blends	J_{sc} (mA/cm^2)	V_{oc} (V)	FF	PCE	R_s (Ωcm^2)	Rsh (Ωcm^2)
3a:PCBM[a]	7.58	0.94	0.38	2.71	61.27	280
3b:PCBM[a]	6.10	1.08	0.34	2.24	78.23	264
3c:PCBM[a]	6.22	1.04	0.34	2.20	74.34	245
3a:PCBM[b]	9.24	0.90	0.48	3.99	48	423
3a:PCBM[c]	10.20	0.90	0.55	5.05	34	510
3c:PCBM[b]	8.52	0.98	0.45	3.56	65	352
3c:PCBM[c]	9.64	0.96	0.52	4.80	52	486

[a]THF cast
[b]TA treatment
[c]TASVA treatment

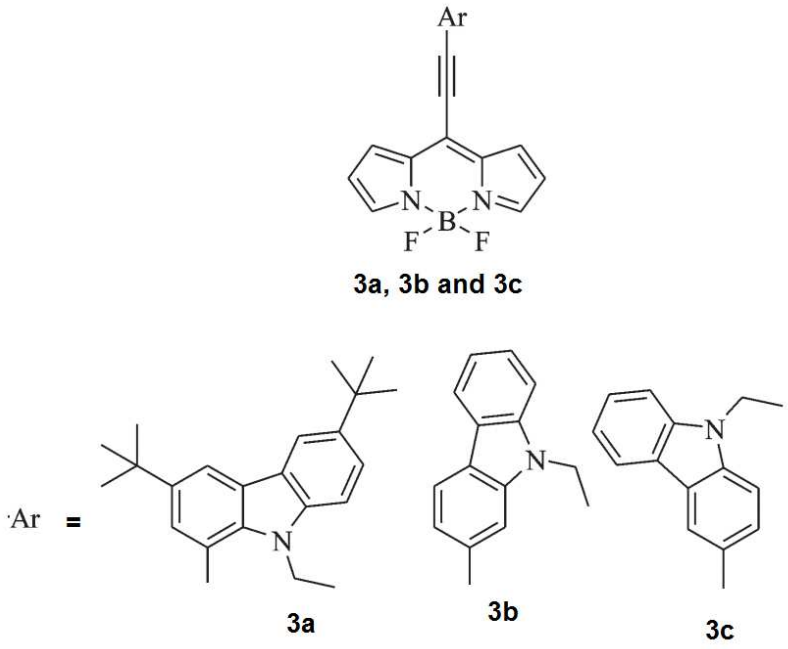

Scheme 1. Chemical structure of **3a**, **3b** and **3c** small molecules.

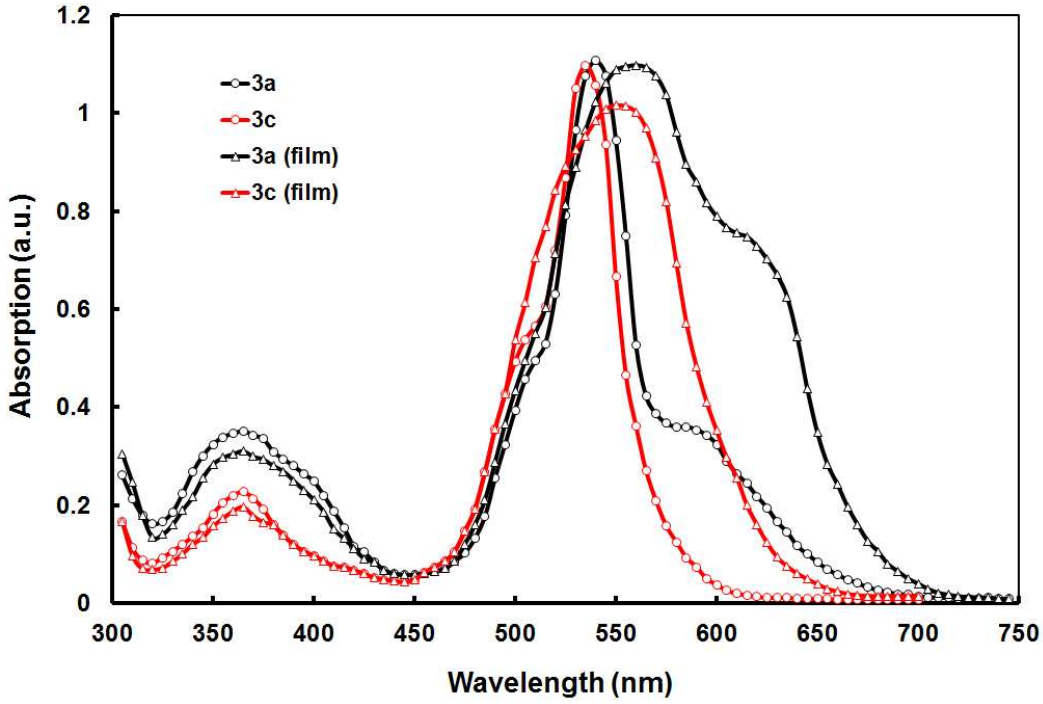

Figure 1. Normalized optical absorption spectra of **3a** and **3c** in DCM solution and thin film cast from DCM.

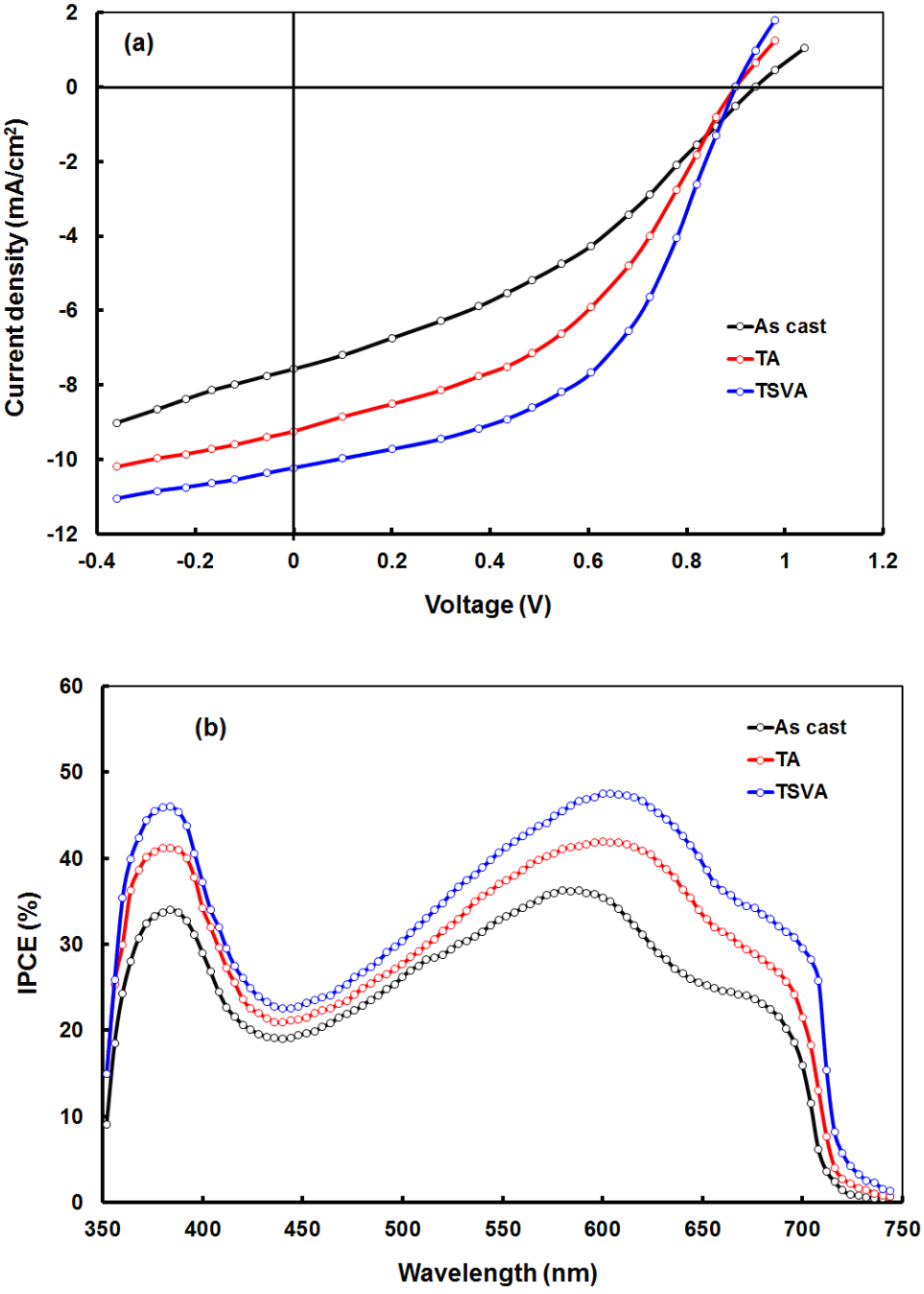

Figure 2. (a) Current –voltage (J-V) characteristics under illumination and (b) IPCE spectra of devices based on **3a**:$PC_{71}BM$ processed under different conditions.

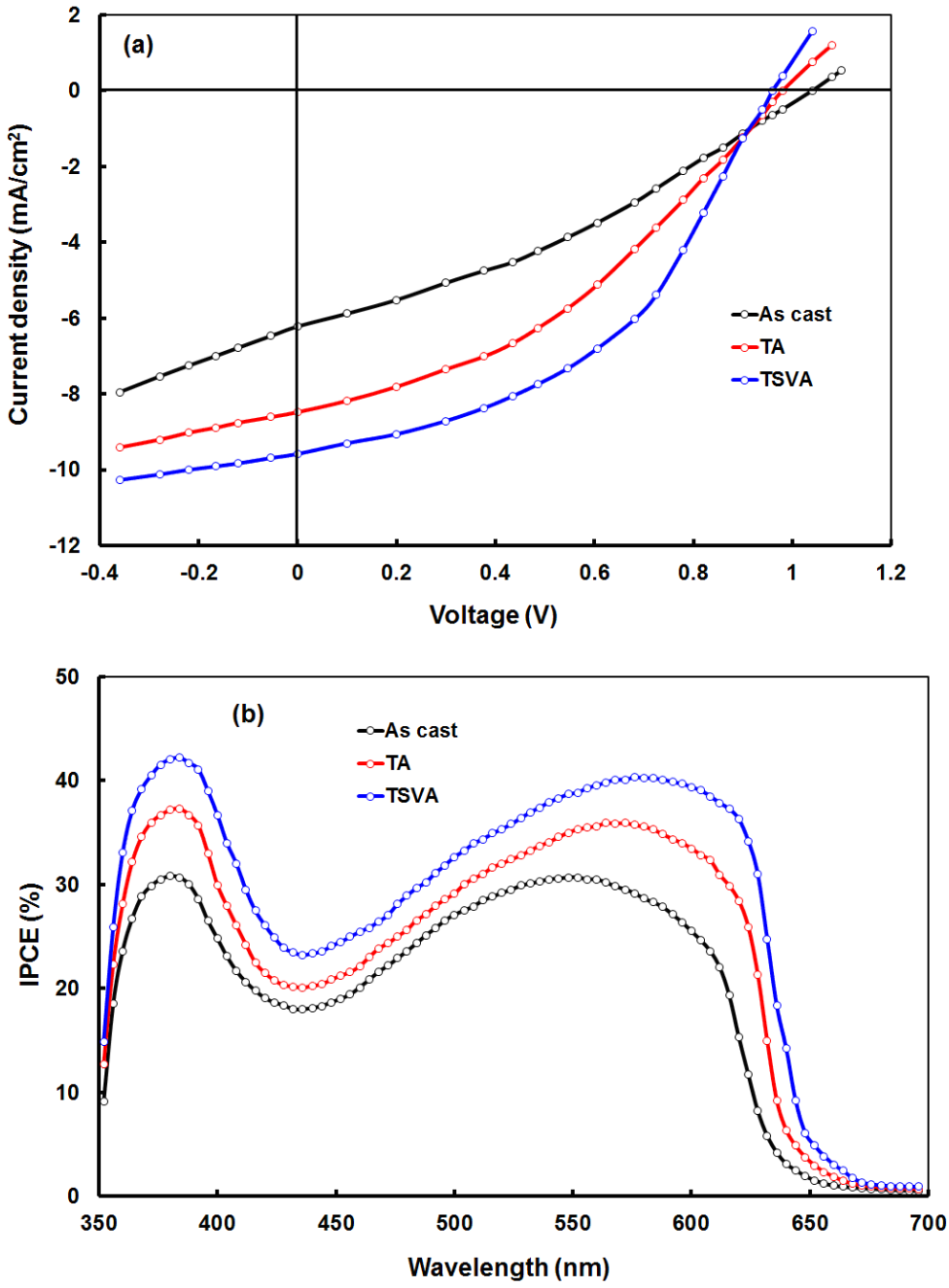

Figure 3. (a) Current –voltage (J-V) characteristics under illumination and (b) IPCE spectra of devices based on **3c**:$PC_{71}BM$ processed under different conditions.

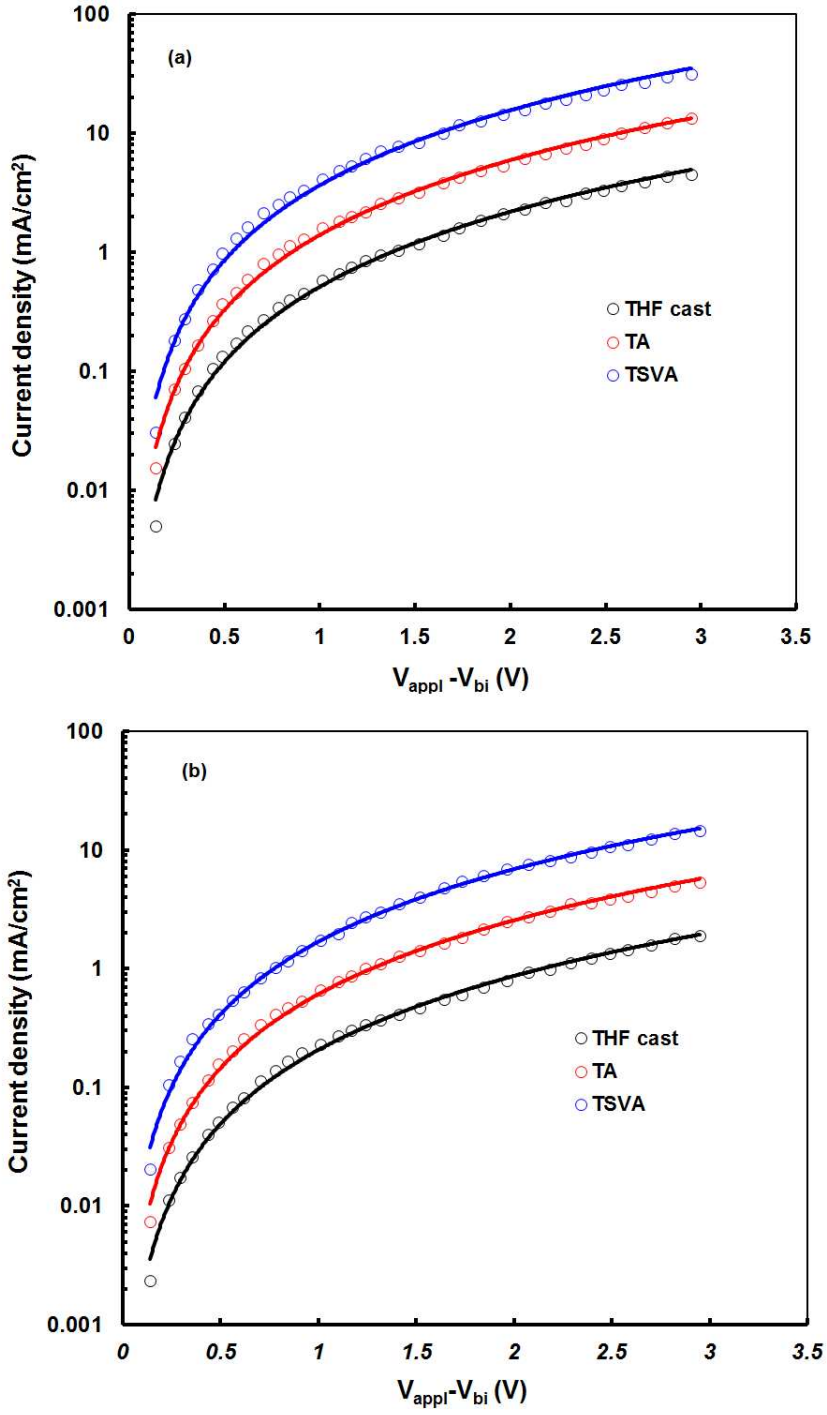

Figure 4. J-V characteristics of hole only devices processed with THF solvent, TA and TSVA treatment active layers for (a) **3a**:$PC_{71}BM$ and (b) **3c** :$PC_{71}BM$. Solid lines are SCLC fitted.

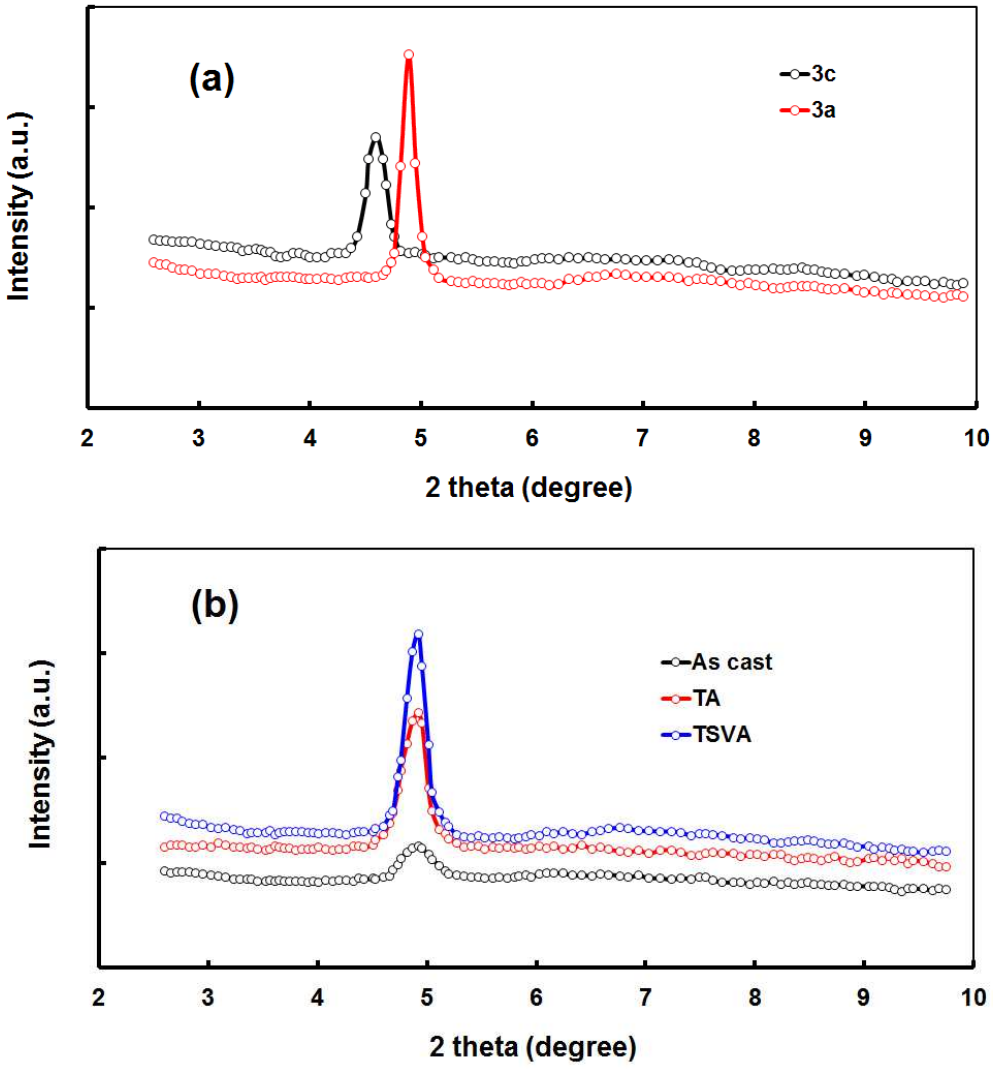

Figure 5. XRD patterns of (a) **3a** and **3c** thin films and (b) **3a**:$PC_{71}BM$ thin films processed under different conditions

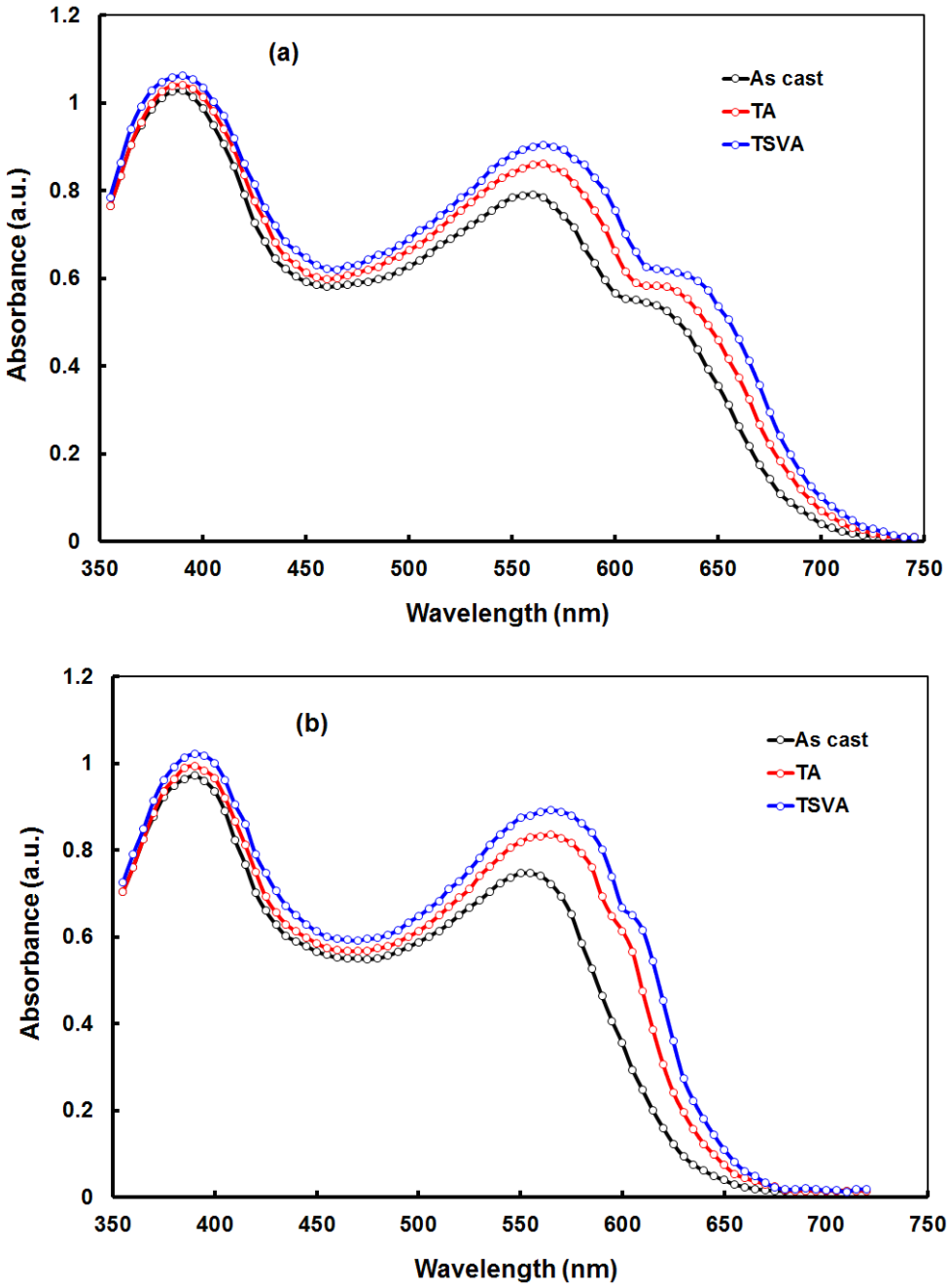

Figure 6. Normalized absorption spectra of as cast THF solution, TA and TSVA treated active layers (a) **3a**:$PC_{71}BM$ and (b) **3c**:$PC_{71}BM$.

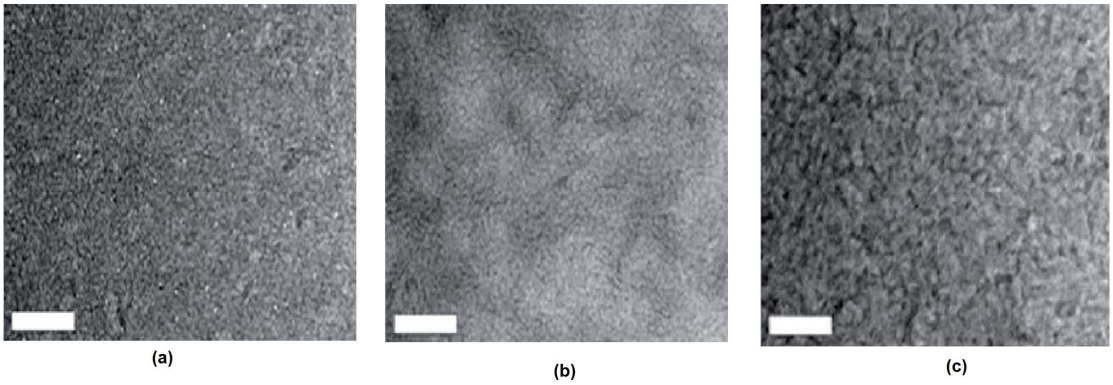

Figure 7. TEM images of active layer **3a**:$PC_{71}BM$ (a) as cast, (b) with TA and (c) TSVA. The scale bar is 200 nm.

TOC

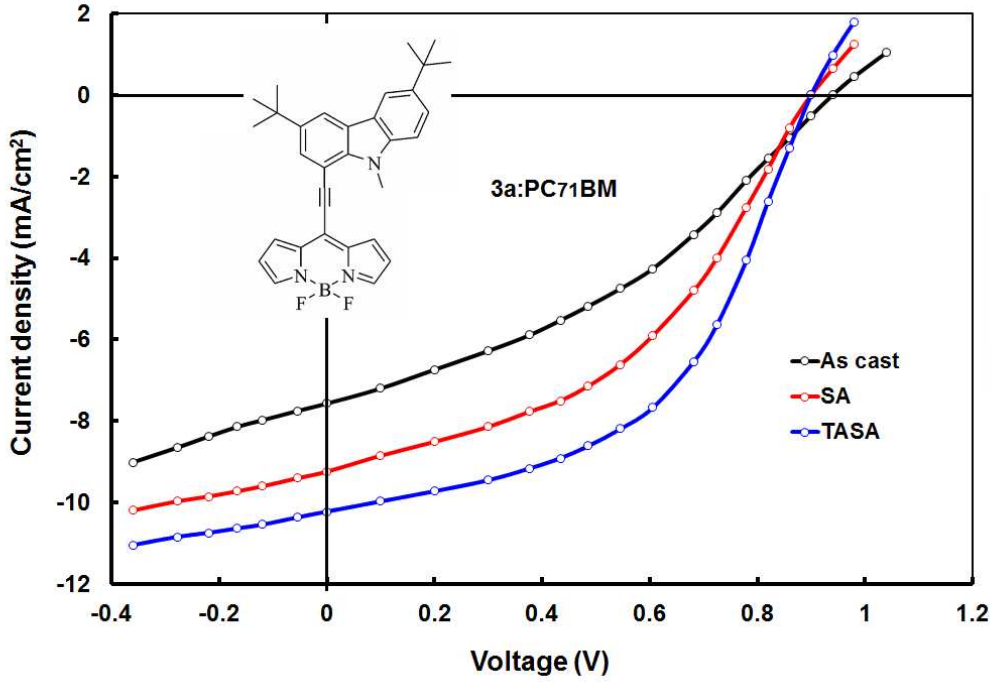

Power conversion efficiency of optimized 3a:$PC_{71}BM$ active layer based device is 5.05%.